

Crystalline electric field excitations in the quantum spin liquid candidate NaYbSe₂

Zheng Zhang^{1,2}, Xiaoli Ma,² Jianshu Li^{1,2}, Guohua Wang,³ D. T. Adroja^{4,5}, T. P. Perring⁴, Weiwei Liu,^{1,2} Feng Jin,² Jianting Ji², Yimeng Wang,^{1,2} Yoshitomo Kamiya³, Xiaoqun Wang³, Jie Ma^{3,*} and Qingming Zhang^{6,2,†}

¹Department of Physics, Renmin University of China, Beijing 100872, China


²Beijing National Laboratory for Condensed Matter Physics, Institute of Physics, Chinese Academy of Sciences, Beijing 100190, China

³Key Laboratory of Artificial Structures and Quantum Control of MOE, Shenyang National Laboratory for Materials Science, Shenyang 110016, China and School of Physics and Astronomy, Tsung-Dao Lee Institute, Shanghai Jiao Tong University, Shanghai 200240, China

⁴ISIS Neutron and Muon Facility, SCFT Rutherford Appleton Laboratory, Chilton, Didcot Oxon OX11 0QX, United Kingdom

⁵Highly Correlated Matter Research Group, Physics Department, University of Johannesburg, P.O. Box 524, Auckland Park 2006, South Africa

⁶School of Physical Science and Technology, Lanzhou University, Lanzhou 730000, China

 (Received 20 February 2020; revised 10 July 2020; accepted 5 January 2021; published 27 January 2021)

By employing inelastic neutron scattering (INS) and Raman scattering (RS) experiments, we comprehensively investigate crystalline electric field (CEF) excitations in NaYbSe₂, a new quantum spin liquid candidate that belongs to a large family of triangular-lattice rare-earth chalcogenides with a high-symmetry structure and negligible structural, spin, and charge disordering effects. We can identify CEF excitations at 15.8, 24.3, and 30.5 meV at 5 K. The selected cuts of the INS spectra are well reproduced with a large anisotropy of $g_{ab} = 2.9$ and $g_c = 1$. The CEF excitations are further confirmed by our calculations based on the point charge model. Interestingly, NaYbSe₂ exhibits an unusual shift of CEF levels to higher energies with increasing temperatures. Further, the Raman mode close to the first CEF excitation shows an anomalously large softening with decreasing temperatures. The absence of these anomalies in the nonmagnetic isostructural material NaLuSe₂ allows us to argue that NaYbSe₂ incorporates an unusually strong CEF-phonon resonancelike coupling not reported in any of the triangular-lattice rare-earth chalcogenides. The determination of the CEF excitations suggests the validity of the picture of an effective spin 1/2 at low temperatures.

DOI: [10.1103/PhysRevB.103.035144](https://doi.org/10.1103/PhysRevB.103.035144)

I. INTRODUCTION

A quantum spin liquid (QSL) is a novel quantum spin-entangled state breaking no symmetry even at zero temperature [1,2]. The idea of QSL was proposed by Anderson in 1973 and then applied to high-temperature superconductivity [3,4]. Since then, many theoretical efforts have been devoted to the exotic state. For instance, Wen proposed a topological classification for QSL based on the parton mean-field theory [5]. Kitaev proposed an exactly solvable spin-1/2 model on the honeycomb lattice, which inspires the idea of topological quantum computing based on the strong spin entanglement of QSL [6].

Extensive efforts have also been made on the material side. Herbertsmithite is a famous QSL candidate with spin-1/2 Cu²⁺ ions on the kagome lattice [7,8], although the antisite mixing between the Cu²⁺ and Zn²⁺ ions remains a key issue in uncovering the intrinsic properties of the ground state. More recently, a topical interest has arisen in materials with strong spin-orbit (SO) coupling. Notably, the rare-earth-based QSL candidate YbMgGaO₂ was discovered, which possesses a perfect spin triangular lattice and rules out the spin impurities and Dyaloshinski-Moriya interaction (DMI) [9]. A series of

experiments down to millikelvin, such as thermodynamic measurements, muon spin relaxation (μ SR), and inelastic neutron scattering (INS), consistently suggest a gapless QSL ground state [10–14]. Meanwhile, it was a concern that the charge disorder between Mg/Ga in YbMgGaO₂ [15] may have an influence on the spin.

By extending the idea of exploring strong SO coupling, we discovered a large family of rare-earth-based QSL candidates, ARECh₂ (A = alkali or monovalent ion, RE = rare earth, Ch = chalcogen) [16]. The family shares the same high symmetry as YbMgGaO₂, inherits almost all the advantages of it, and naturally resolves the issue of charge disorder. Remarkably, preliminary results on various compounds in the large family show the enhanced antiferromagnetic (AF) exchange coupling compared to YbMgGaO₂. These advantages render the family as an ideal playground for spin liquid study.

NaYbCh₂ is the subfamily of rare-earth chalcogenides for which research efforts are rapidly accumulating [16–24]. In particular, NaYbSe₂ attracts much interest because of its distinct signature of a QSL and the charge gap ($\simeq 1.92$ eV) that is appropriate for material engineering such as pressure-induced metallization [16,25]. And even unconventional superconductivity has been reported [25]. To investigate the magnetic properties at low temperatures, the influence of the ligand anions on structural properties, etc., precise knowledge of the crystalline electric field (CEF) excitations is essential. It is

*jma3@sjtu.edu.cn

†qmzhang@ruc.edu.cn

also noteworthy that we are already able to grow large single crystals of NaYbSe₂ (with the largest dimension $\simeq 20$ mm) that are adequate for an INS study. Our study of CEF excitations is essential to pave the way for investigating the magnetic ground-state properties by using INS measurements.

In this paper, by performing INS and Raman scattering (RS) measurements on NaYbSe₂ and its nonmagnetic reference compound NaLuSe₂, we comprehensively investigated the CEF excitations in NaYbSe₂ and revealed an unusual CEF-phonon resonancelike coupling. We identify three CEF excitations, at 15.79, 24.33, and 30.53 meV, by INS experiments at 5 K, which are also confirmed by RS experiments. Our analysis based on a CEF Hamiltonian well reproduces the selected cuts of the INS spectra. We also employed the point charge model to calculate the CEF excitations, which are basically consistent with our experiments [26], particularly the lowest ones. Both INS and RS experiments demonstrate that the CEF excitations exhibit an unusual shift to higher energies with increasing temperatures. The Raman mode very close to the first CEF excitation is significantly softened with decreasing temperatures accompanying an unusual behavior also in linewidth. The fact that these anomalies are completely absent in NaLuSe₂ allows us to identify a CEF-phonon resonancelike coupling in NaYbSe₂. The phonon anomalies as well as the unusual CEF temperature dependence can be explained in terms of the electronegativity of chalcogen elements.

II. EXPERIMENTAL TECHNIQUES

The high-quality single crystals of NaYbSe₂, as well as the nonmagnetic NaLuSe₂, were grown using a NaCl-flux method. The single crystals with the dimensions of 5×5 mm were used in the RS experiments. The polycrystalline samples of NaYbSe₂ and NaLuSe₂ were synthesized by the high-temperature solid-state reaction and were characterized to be single phased [16]. The polycrystalline samples of NaYbSe₂ ($\simeq 5$ g) and NaLuSe₂ ($\simeq 3$ g) were used in the INS experiments [26]. The INS data on NaYbSe₂ and nonmagnetic reference compound NaLuSe₂ were collected using the high-flux and high-resolution time-of-flight spectrometers, MAPS, at the ISIS pulsed neutron facility, Rutherford Appleton Laboratory, United Kingdom. The instrumental full width at half maxima (FWHM) is ~ 1.48 meV. The polycrystalline samples were loaded in an Al can with an inner diameter of 30 mm. The closed-cycle refrigerator (CCR) was used to cool the samples to a base temperature of 5 K with He-exchange gas. Finally, the energy and temperature dependence of the data were obtained. The Raman spectra were collected using a HR800 (Jobin Yvon) and T64000 (Jobin Yvon) equipped with a 633 nm and 473 nm laser, charge-coupled device (CCD), and volume Bragg gratings. After cleavage, the single crystals of NaYbSe₂ and NaLuSe₂ were placed in a closed-cycle cryostat for the Raman experiments. A backscattering configuration was employed and the polarizations of both the incident and scattering light lie in the single-crystal *ab* plane.

III. CEF EXCITATIONS AND INELASTIC NEUTRON SCATTERING

The INS spectra for NaYbSe₂ with the incident neutron energies $E_i = 19.3, 27.7, 50.0, 70.0,$ and 150.0 meV at 5 K are

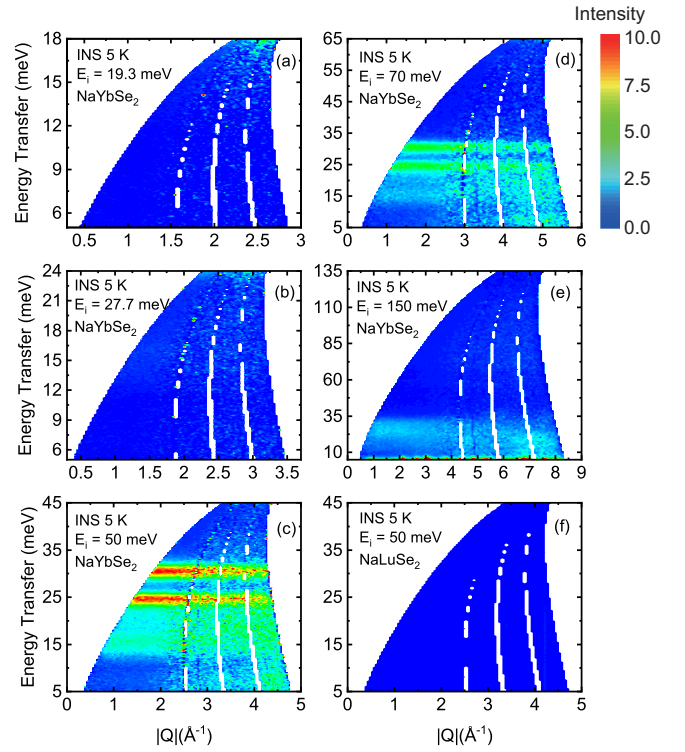


FIG. 1. (a)–(e) The INS spectra of NaYbSe₂ measured with increasing incident neutron energies at 5 K. For comparison, (f) is the INS spectrum of NaLuSe₂ measured with an incident energy of 50.0 meV at 5 K. The intensity color scale of NaLuSe₂ has been normalized to NaYbSe₂.

shown in Fig. 1. Three excitations can be seen at 15.8, 24.3, and 30.5 meV in Figs. 1(c) and 1(d). In conjunction with the observation that the excitations in NaYbSe₂ are momentum independent, we conclude that they are not due to phonons but unambiguously of the CEF origin. For comparison, the INS spectra of nonmagnetic reference sample NaLuSe₂ are also measured and no momentum-independent CEF excitation is observed. At the same time, in the INS spectra of NaLuSe₂, a weaker excitation peak can be observed near 17 meV [26], and it moves to lower energy with increasing temperatures [26]. Our RS experiments (see below) further identify the corresponding CEF excitations in NaYbSe₂ and demonstrate that the weak excitation in the INS spectra of NaLuSe₂ belongs to the E_g mode phonon.

In particular, the first CEF excitation sets a fundamental energy scale for studying the magnetism of NaYbSe₂ and is the key to look into various thermodynamic behaviors at elevated temperatures, including the Curie-Weiss one.

Figure 2 demonstrates the temperature dependence of the CEF excitations. The cuts of the integrated spectra in the ranges of low wave vector ($\sim 0 - 3 \text{ \AA}^{-1}$) and high wave vector ($\sim 3 - 5 \text{ \AA}^{-1}$) are shown in Figs. 2(f)–2(j) and Figs. 2(k)–2(o). The red dashed lines in Fig. 2 mark the center peak positions of CEF excitations based on the fitting of the cuts of the INS spectra. The green dashed lines in Fig. 2 mark the E_g mode phonon excitation observed in the cuts of the INS spectra above 100 K and can be confirmed by RS experiments. There are several points we can draw from Fig. 2.

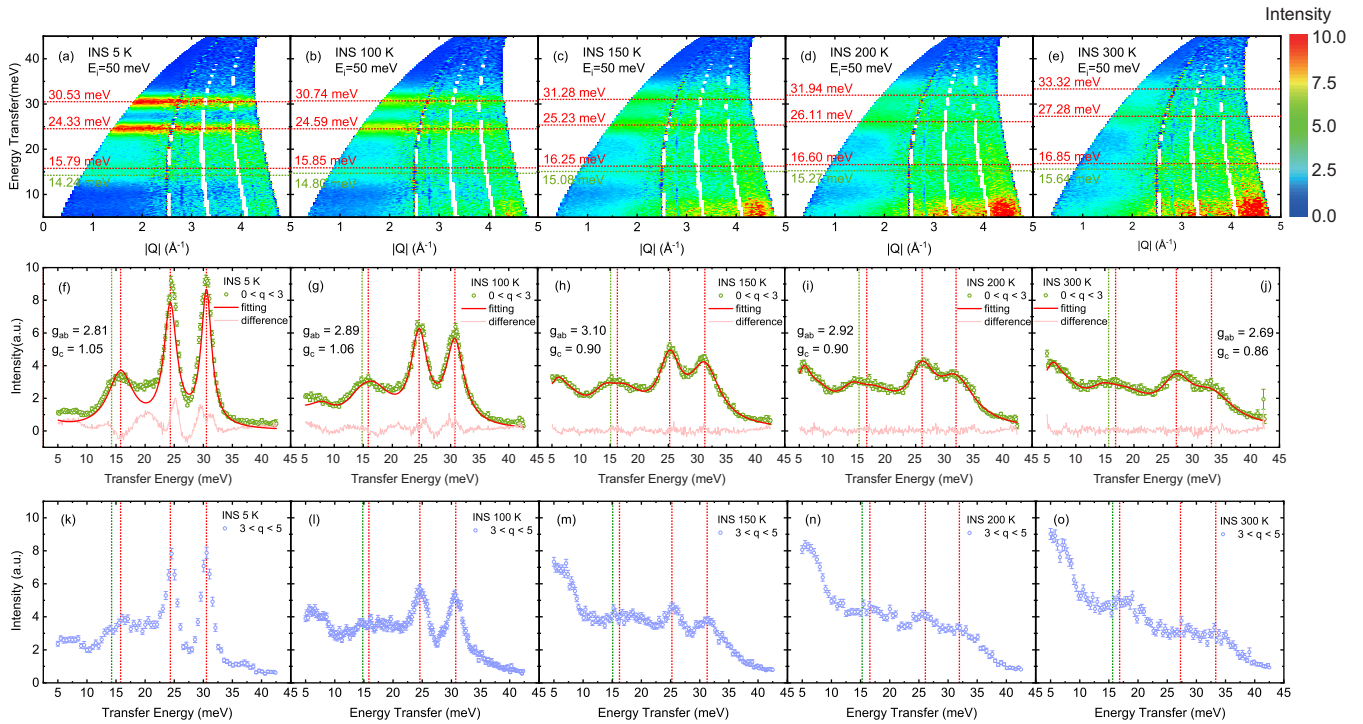


FIG. 2. (a)–(e) The INS spectra of NaYbSe₂ measured with the incident neutron energy $E_i = 50$ meV at selected temperatures. (f)–(j) The cuts of INS intensity vs energy at five temperatures. The data in (f)–(j) and (k)–(o) have been integrated over the wave-vector space from 0 to 3 Å⁻¹ (green dots) and 3 to 5 Å⁻¹ (purple dots). The fitting curves (red lines) were obtained using the standard program in MANTID [27]. In (a)–(e) and (f)–(j), the first, second, and third CEF excitations of Yb³⁺ are highlighted by red dashed lines and the E_g mode phonon excitation in NaYbSe₂ is highlighted by green dashed lines.

(i) The intensity of the three CEF excitations decreases with $|Q|$. This can be explained by the magnetic form factor $F(|Q|)$ in the differential neutron scattering cross section. By calculating $F^2(|Q|)$ as a function of $|Q|$, we found that the scattering intensity decreases with increasing $|Q|$, consistent with the observation here [26].

(ii) The intensity of the CEF excitations decreases with increasing temperatures. This simply comes from the thermal broadening and population factor, and similar behavior has also been seen in YbMgGaO₂ [15].

(iii) Most interestingly, the CEF excitations exhibit a slight but clear shift to higher energies with increasing temperatures. Our Raman experiments also detect the shift (Fig. 4). This unusual temperature dependence was observed in neither YbMgGaO₂ [15] nor NaYbS₂ [28]. The temperature-dependent CEF excitations are quite unusual. This seems related to the larger radius of Se anion or its weaker electronegativity. At lower temperatures, there is a larger overlap of electron cloud between Yb and Se, which reduces the effective charges of the Se anions and hence gives rise to the lower CEF levels. With increasing the temperatures, the thermal lattice expansion normally slightly enlarges the bond distance between Yb and Se and reduces the electron cloud overlap between them. Consequently, this slightly enhances the ionicity of the compound and raises the effective charge of Se, which eventually raises the CEF levels by a small amount. Thermal broadening of the CEF levels at higher temperatures makes the shift obscure, as observed in neutron experiments. We can check the existing CEF INS experimental data of NaYbO₂ [17] and NaYbS₂ [28] which support the explanation of electronegativity. The first CEF excitation energy levels of NaYbSe₂, NaYbS₂, and NaYbO₂ increase in sequence, while the electronegativity of Se, S, and O increases in sequence. In addition, the CEF-phonon resonancelike coupling (see below) may further enhance the

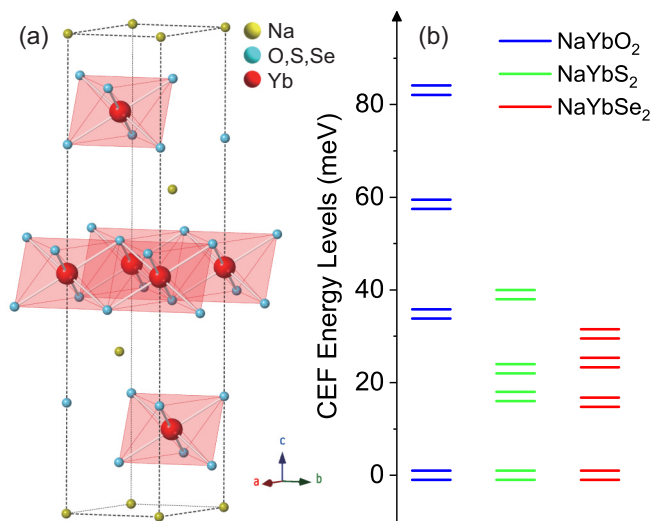


FIG. 3. (a) Crystal structure of NaYbCh₂ (Ch=O, S, Se). (b) Experimental CEF excitation energy levels extracted from INS experiments [17,28].

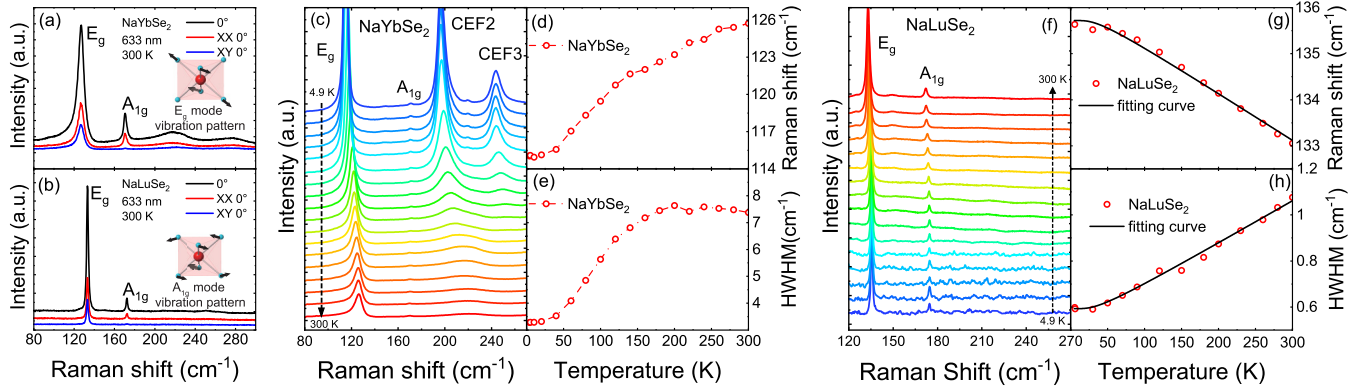


FIG. 4. Raman spectra for NaYbSe₂ and NaLuSe₂. (a),(b) The NaYbSe₂ and NaLuSe₂ polarized Raman spectrum at 300 K, respectively. XX and XY represent parallel and cross polarization configurations, respectively. The insets of (a) and (b) show the vibration patterns of the E_g and A_{1g} phonon modes. (c),(f) The temperature evolution of Raman spectra in NaYbSe₂ and NaLuSe₂, respectively. The Raman shifts and the half widths at half maximum (HWHM) of the E_g mode are shown in (d), (e), (g), and (h).

character of the CEF excitations shift to higher energies with increasing temperatures.

(iv) The offset of the first CEF excitation energy level ($\Delta E = E_{300K} - E_{5K} = 1.06$ meV) with increasing temperatures is smaller than the second ($\Delta E = E_{300K} - E_{5K} = 2.95$ meV) and third ($\Delta E = E_{300K} - E_{5K} = 2.79$ meV) ones in Fig. 2. The CEF-phonon coupling enables an energy exchange between the first CEF excitation and phonons, and may be responsible for the smaller shift of the first CEF excitation.

We used the standard spectral analysis program [27] (MAN-TID) to determine the CEF parameters by fitting the cuts of the INS spectra in the range from 0 to 3 Å⁻¹. The fitting details and the extracted CEF parameters can be found in the Supplemental Material [26]. The g factors given by the fittings have the ratio of g_{ab} to g_c around 3:1 [Figs. 2(f)–2(j)], which is close to that in NaYbO₂ and NaYbS₂ [29]. This indicates that the subfamily AYbCh₂ has a systematic and strong magnetic anisotropy, which is in stark contrast within YbMgGaO₂, where the ratio is close to 1 [10]. The difference may stem from the charge imbalance of different cations between the Yb³⁺ layers [29].

We have also calculated the CEF levels in NaYbO₂, NaYbS₂, and NaYbSe₂ using the point charge model [26] and made a comparison with the existing INS data [Fig. 3(b)]. Generally, the CEF levels decrease with the increase of ion radii, i.e., in the order of O, S, and Se, as expected. One can see an agreement between experiments and calculations for the first CEF level. The calculated first CEF levels are ~ 39.7 meV (NaYbO₂), ~ 20.2 meV (NaYbS₂), and ~ 16.52 meV (NaYbSe₂) [26], and the experimental values obtained from the INS measurements are 34.8 meV [17], 17.0 meV [28], and 15.8 meV, respectively. It implies that the ionic crystal picture still works in the case of larger selenium anions. When we look at the second and third excitation levels, there is a relatively large discrepancy between the experimental and calculated ones. The discrepancy is related to the simplification of the anisotropic orbitals in the point charge model. It means that we need to go beyond the first-order isotropic s -orbital picture if we want to accurately calculate higher CEF energy levels. On the other hand, the lowest CEF

excitation rather than the higher CEF energy levels plays a key role in the low-energy physics which we are concerned with.

IV. CEF-PHONON RESONANCE-LIKE COUPLING AND RAMAN SCATTERING

Figure 4 shows the Raman spectra of NaYbSe₂ and NaLuSe₂. The crystal symmetry of $R\bar{3}m$ allows two Raman-active phonon modes $A_g + E_g$. Symmetry analysis indicates that the A_g mode is visible only in the parallel polarization configuration, while the E_g mode can be observed in both parallel and cross polarization configurations. The two modes can be clearly identified with the polarized spectra in Figs. 4(a) and 4(b). Meanwhile, the E_g phonon mode of NaYbSe₂ (marked by the green dashed lines in Fig. 2) and NaLuSe₂ [26] can also be observed in the INS spectra.

Besides the Raman modes, two weaker bands appear at 217 cm⁻¹ (≈ 26.9 meV) and 277 cm⁻¹ (≈ 33.3 meV) in NaYbSe₂. The frequencies exactly match the second and third CEF energy levels observed in the INS measurements. The two bands can be assigned to the CEF excitations since they completely disappear in NaLuSe₂. Actually, Raman scattering is a unique method to probe CEF excitations and has been applied to many rare-earth-based spin systems such as Tb₂Ti₂O₇ [30–32]. It is worth noting that the intensities of the two bands are quite different in the parallel and cross polarization configurations [Figs. 4(a) and 4(b)]. This may be related to the strong anisotropy in NaYbSe₂. We did not observe the feature corresponding to the first CEF level in the RS spectra. A possible reason is that the first CEF excitation of 16 meV (≈ 185 K) is weaker and broader (FWHM ≈ 10 meV) than the second (FWHM ≈ 5 meV) and third (FWHM ≈ 5 meV) CEF excitations in the INS experiments.

There are several evident anomalies in the Raman spectra of NaYbSe₂, including phonon mode broadening, asymmetric line shape of the E_g mode, a large softening of the E_g mode [Fig. 4(d)], and unusual temperature dependence of its width [Fig. 4(e)]. The anomalies are absent in the nonmagnetic reference compound NaLuSe₂. The spin-phonon coupling seems unlikely to be responsible for the anomalies because

the broadening and asymmetry of the E_g mode already exist even at room temperature, which is larger by almost an order of magnitude than the exchange coupling. Furthermore, the inversion center between adjacent magnetic ions prohibits the first-order spin-phonon coupling and the system remains spin disordered down to the lowest measurement temperatures. On the other hand, the phonon mode (E_g) very close to the first CEF excitation in energy (less than 1 meV) has been identified by our Raman and INS spectra in NaYbSe₂ and NaLuSe₂. The phonon mode exhibits a large softening with decreasing temperatures. This is a clear indication of the coupling between the mode and the lowest excitation. The strong coupling should give rise to a significant damping for both the phonon mode and the lowest excitation. Thus we can identify that the anomalies are due to the CEF-phonon coupling. As a matter of fact, the CEF-phonon coupling has been reported in some rare-earth compounds [30,32,33]. It may provide an alternative possibility to tune the CEF excitations and the magnetism of the rare-earth spin system.

Compared to Yb-O and Yb-S, Yb-Se has a larger electron cloud overlap, which, in principle, gives rise to a CEF-phonon coupling. The coupling in NaYbSe₂ is remarkably enhanced by the resonancelike effect between the first CEF excitation and the E_g mode. More precisely, the first CEF excitation is only ~ 1 meV higher than the phonon energy at room temperature. With decreasing temperatures, the phonon frequency normally goes up while the first CEF level goes down, as discussed above. The tiny energy discrepancy will be easily compensated and the resonancelike effect occurs. Generally, the effect splits the resonance energy into the lower (phonon) and upper (CEF) branches and the temperature-dependent INS experiments of NaYbSe₂ (Fig. 2) are consistent with this picture.

V. CONCLUSION

We studied the CEF excitations of Yb³⁺ in NaYbSe₂ using INS and RS experiments and by comparison with nonmagnetic reference sample NaLuSe₂. We observed three CEF excitations by INS experiments and extracted the CEF parameters by fitting the cuts of the INS spectra. We used the point charge model to reproduce the CEF excitations of

NaYbO₂, NaYbS₂, and NaYbSe₂, among which the lowest CEF levels show a better consistence with the experimental observations.

NaYbSe₂ exhibits some unique features in the CEF excitations compared to NaYbO₂ and NaYbS₂. First, the observed CEF excitations exhibit an unusual shift to higher energies with increasing temperatures. This is naturally understood in terms of electronegativity. Second, the material has a strong CEF-phonon coupling. The comparison of the INS spectra of NaYbSe₂ and NaLuSe₂ allows us to identify a phonon mode around 15 meV, which is very close to the first CEF excitation of NaYbSe₂. The CEF excitations and the phonon mode are further confirmed in the Raman scattering experiments. Surprisingly, the E_g mode phonon close to the first CEF excitation shows a large softening with decreasing temperatures, while the same mode in NaLuSe₂ has a normal hardening. The contrast is a clear demonstration of the CEF-phonon resonancelike coupling. “Resonancelike” means that the E_g mode phonon and the first CEF level are very close in energy (about 1 meV), and the “coupling” is reflected in the energy exchange between the E_g mode phonon and the first CEF energy level.

ACKNOWLEDGMENTS

This work was supported by the National Key Research and Development Program of China (Grants No. 2017YFA0302904 and No. 2016YFA0300500), the NSF of China (Grants No. U1932215 and No. 11774419), and the Strategic Priority Research Program of the Chinese Academy of Sciences (Grant No. XDB33010100). X.Q.W. is supported by NSFC, Grant No. 11974244 and a Shanghai talent program. Y.K. acknowledges the support from the NSFC Research Fund (Grants No. 11950410507 and No. 12074246). We thank the ISIS Facility for beam time and data can be obtained at Dr J. Ma *et al.* [44]. The data processing of the INS spectrum in Figs. 1 and 2 are based on the MANTID software [27]. The CEF energy levels and g -factor calculation are based on MathWorks MATLAB (Academic License for Renmin University of China) software. The theoretical calculation of CEF based on the point charge model is also based on the MANTID software [27].

-
- [1] L. Balents, *Nature (London)* **464**, 199 (2010).
 - [2] L. Savary and L. Balents, *Rep. Prog. Phys.* **80**, 016502 (2016).
 - [3] P. W. Anderson, *Mater. Res. Bull.* **8**, 153 (1973).
 - [4] P. W. Anderson, *Science* **235**, 1196 (1987).
 - [5] X. G. Wen, *Phys. Rev. B* **44**, 2664 (1991).
 - [6] A. Kitaev, *Ann. Phys.* **321**, 2 (2006).
 - [7] M. P. Shores, E. A. Nytko, B. M. Bartlett, and D. G. Nocera, *J. Am. Chem. Soc.* **127**, 13462 (2005).
 - [8] T.-H. Han, J. S. Helton, S. Chu, D. G. Nocera, J. A. Rodriguez-Rivera, C. Broholm, and Y. S. Lee, *Nature (London)* **492**, 406 (2012).
 - [9] Y. Li, H. Liao, Z. Zhang, S. Li, F. Jin, L. Ling, L. Zhang, Y. Zou, Li. Pi, Z. Yang, and Q. Zhang, *Sci. Rep.* **5**, 16419 (2015).
 - [10] Y. Li, G. Chen, W. Tong, Li. Pi, J. Liu, Z. Yang, X. Wang, and Q. Zhang, *Phys. Rev. Lett.* **115**, 167203 (2015).
 - [11] Y. Li, D. Adroja, P. K. Biswas, P. J. Baker, Q. Zhang, J. Liu, A. A. Tsirlin, P. Gegenwart, and Q. Zhang, *Phys. Rev. Lett.* **117**, 097201 (2016).
 - [12] Y. Li, D. Adroja, D. Voneshen, R. I. Bewley, Q. Zhang, A. A. Tsirlin, and P. Gegenwart, *Nat. Commun.* **8**, 1 (2017).
 - [13] Y. Shen, Y.-D. Li, H. Wo, Y. Li, S. Shen, B. Pan, Q. Wang, H. C. Walker, P. Steffens, M. Boehm, Y. Hao, D. L. Quintero-Castro, L. W. Harriger, M. D. Frontzek, L. Hao, S. Meng, Q. Zhang, G. Chen, and J. Zhao, *Nature (London)* **540**, 559 (2016).
 - [14] Y. Li, *Adv. Quantum Technol.* **2**, 1900089 (2019).
 - [15] Y. Li, D. Adroja, R. I. Bewley, D. Voneshen, A. A. Tsirlin, P. Gegenwart, and Q. Zhang, *Phys. Rev. Lett.* **118**, 107202 (2017).

- [16] W. Liu, Z. Zhang, J. Ji, Y. Liu, J. Li, X. Wang, H. Lei, G. Chen, and Q. Zhang, *Chin. Phys. Lett.* **35**, 117501 (2018).
- [17] L. Ding, P. Manuel, S. Bachus, F. Grubler, P. Gegenwart, J. Singleton, R. D. Johnson, H. C. Walker, D. T. Adroja, A. D. Hillier, and A. A. Tsirlin, *Phys. Rev. B* **100**, 144432 (2019).
- [18] K. M. Ranjith, S. Luther, T. Reimann, B. Schmidt, P. Schlender, J. Sichelschmidt, H. Yasuoka, A. M. Strydom, Y. Skourski, J. Wosnitza, H. Kühne, T. Doert, and M. Baenitz, *Phys. Rev. B* **100**, 224417 (2019).
- [19] J. Xing, L. D. Sanjeeva, J. Kim, G. R. Stewart, M.-H. Du, F. A. Reboredo, R. Custelcean, and A. S. Sefat, *ACS Mater. Lett.* **2**, 71 (2019).
- [20] M. M. Bordelon, E. Kenney, C. Liu, T. Hogan, L. Posthuma, M. Kavand, Y. Lyu, M. Sherwin, N. P. Butch, C. Brown, M. J. Graf, L. Balents, and S. D. Wilson, *Nat. Phys.* **15**, 1058 (2019).
- [21] J. Xing, L. D. Sanjeeva, J. Kim, W. R. Meier, A. F. May, Q. Zheng, R. Custelcean, G. R. Stewart, and A. S. Sefat, *Phys. Rev. Materials* **3**, 114413 (2019).
- [22] J. Xing, L. D. Sanjeeva, J. Kim, G. R. Stewart, A. Podlesnyak, and A. S. Sefat, *Phys. Rev. B* **100**, 220407(R) (2019).
- [23] S. Gao, F. Xiao, K. Kamazawa, K. Ikeuchi, D. Biner, K. Krämer, C. Rüegg, and T.-H. Arima, *Phys. Rev. B* **102**, 024424 (2020).
- [24] J. Ma, J. Li, Y. H. Gao, C. Liu, Q. Ren, Z. Zhang, Z. Wang, R. Chen, J. Embs, E. Feng, F. Zhu, Q. Huang, Z. Xiang, Lu. Chen, E. S. Choi, Z. Qu, Lu. Li, J. Wang, H. Zhou, Y. Su, X. Wang, Q. Zhang, and G. Chen, [arXiv:2002.09224v1](https://arxiv.org/abs/2002.09224v1).
- [25] Z. Zhang, Y. Yin, X. Ma, W. Liu, J. Li, F. Jin, J. Ji, Y. Wang, X. Wang, X. Yu, and Q. Zhang, [arXiv:2003.11479v1](https://arxiv.org/abs/2003.11479v1).
- [26] See Supplemental Material at <http://link.aps.org/supplemental/10.1103/PhysRevB.103.035144> for sample preparation and characterization, analysis of neutron scattering and Raman scattering, and point charge model, which includes Refs. [10,16,27,28,34–43].
- [27] O. Arnold, J. C. Bilheux, J. M. Borreguero, A. Buts, S. I. Campbell, L. Chapon, M. Doucet, N. Draper, R. F. Leal, M. A. Gigg, V. E. Lynch, A. Markvardsen, D. J. Mikkelsen, R. L. Mikkelsen, R. Miller, K. Palmen, P. Parker, G. Passos, T. G. Perring, P. F. Peterson, S. Ren, M. A. Reuter, A. T. Savici, J. W. Taylor, R. J. Taylor, R. Tolchenov, W. Zhou, and J. Zikovsky, *Nucl. Instrum. Methods Phys. Res. A* **764**, 156 (2014).
- [28] M. Baenitz, P. Schlender, J. Sichelschmidt, Y. A. Onykienko, Z. Zangeneh, K. M. Ranjith, R. Sarkar, L. Hozoi, H. C. Walker, J.-C. Orain, H. Yasuoka, J. van den Brink, H. H. Klauss, D. S. Inosov, and T. Doert, *Phys. Rev. B* **98**, 220409(R) (2018).
- [29] Z. Zangeneh, S. Avdoshenko, J. van den Brink, and L. Hozoi, *Phys. Rev. B* **100**, 174436 (2019).
- [30] G. Güntherodt, A. Jayaraman, G. Batlogg, M. Croft, and E. Melzer, *Phys. Rev. Lett.* **51**, 2330 (1983).
- [31] M. Maczka, M. L. Sanjuán, A. F. Fuentes, K. Hermanowicz, and J. Hanuza, *Phys. Rev. B* **78**, 134420 (2008).
- [32] A. Sethi, J. E. Slimak, T. Kolodiazny, and S. L. Cooper, *Phys. Rev. Lett.* **122**, 177601 (2019).
- [33] K. Hense, E. Gratz, H. Nowotny, and A. Hoser, *J. Phys. Condens. Matter* **16**, 5751 (2004).
- [34] T. Schleid and F. Lissner, *Eur. J. Sol. Stat. Inorg. Chem* **30**, 829 (1993).
- [35] A. Bertin, Y. Chapuis, P. D. de Réotier, and A. Yaouanc, *J. Phys. Condens. Matter* **24**, 256003 (2012).
- [36] D. J. Newman and B. Ng, *Crystal Field Handbook* (Cambridge University Press, Cambridge, 2007).
- [37] I. Mirebeau, P. Bonville, and M. Hennion, *Phys. Rev. B* **76**, 184436 (2007).
- [38] M. Ruminy, E. Pomjakushina, K. Iida, K. Kamazawa, D. T. Adroja, U. Stuhr, and T. Fennell, *Phys. Rev. B* **94**, 024430 (2016).
- [39] E. Prince, *International Tables for Crystallography: Volume C* (Kluwer Academic, Norwell, MA, 2004).
- [40] O. Arnold, A. Bamidele, L. Basso, J. Borreguero, E. Brown, H. Brown, N. Draper, M. Ganeva, M. A. Gigg, G. Guest, S. Hahn, S. Heybrock, A. J. Jackson, S. Jenkins, S. Jones, D. Le, R. Leal, A. Lim, J. Lin, V. Lynch, M. McDonnell, G. Miladinovic, L. Moore, D. Nixon, E. Oram, P. F. Peterson, V. Reimund, A. Russell, H. Saunders, A. Savici, A. Soininen, A. Sokolova, B. Sullivan, D. Tasev, T. Titcombe, R. Tolchenov, G. Vardanyan, R. Whitfield, M. Andrew, R. Applin, and W. Zhou, Mantid 4.1.0: Manipulation and analysis toolkit for instrument data, (Mantid Project, 2019), <http://dx.doi.org/10.5286/SOFTWARE/MANTID>.
- [41] J. J. Baldoví, S. Cardona-Serra, J. M. Clemente-Juan, E. Coronado, A. Gaita-Ariño, and A. Palií, *J. Comput. Chem.* **34**, 1961 (2013).
- [42] H. Wondratschek and U. Muller, *International Tables for Crystallography, Volume A1* (Kluwer Academic, Norwell, MA, 2004).
- [43] D. L. Rousseau, R. P. Bauman, and S. P. S. Porto, *J. Raman Spectrosc.* **10**, 253 (1981).
- [44] J. Ma, Q. Zhang, and D. Adroja, Inelastic neutron study to investigate the crystal electronic field of rare-earth chalcogenides NaReSe₂ (Re = Yb and Er) (2019), <https://doi.org/10.5286/ISIS.E.RB1910575>.